International Journal of Thermal Sciences 58 (2012) 120–129

Contents lists available at SciVerse ScienceDirect

International Journal of Thermal Sciences

journal homepage: www.elsevier.com/locate/ijts

Heat transfer performance and hydrodynamic behavior of turbulent nanofluid radial flows

Gilles Roy [a,*], Iulian Gherasim [b], François Nadeau [a], Gérard Poitras [a], Cong Tam Nguyen [a]

[a] Faculty of Engineering, Université de Moncton, Moncton, NB, E1A 3E9, Canada
[b] Department of Building Services, Faculty of Civil Engineering and Building Services, Technical University "Gheorghe Asachi", 45A Mangeron, 700050 Iasi, Romania

ARTICLE INFO

Article history:
Received 25 October 2011
Received in revised form
14 March 2012
Accepted 14 March 2012
Available online 22 April 2012

Keywords:
Turbulent radial flow
Nanofluids
Confined radial flow
Heat transfer enhancement
Pumping power
Nanofluid performance
Performance evaluation criterion
CFD
Numerical investigation

ABSTRACT

This paper presents a numerical investigation of heat transfer and hydrodynamic behavior of various types of water-based nanofluids inside a typical radial flow cooling device. Turbulent radial nanofluid flow between two parallel disks with axial injection is considered. Several turbulence models were evaluated. The RANS-based $\kappa - \omega$ SST turbulence model was chosen for subsequent simulations. A single phase fluid approach was used throughout with temperature dependant nanofluid effective properties. Results show that although heat transfer enhancement is found for all types of nanofluids considered, energy-based performance comparisons indicate that they do not necessarily represent the most efficient coolants for this type of application and flow conditions.

1. Introduction

Nanoparticle suspensions (i.e. nanofluids) have generated an impressive amount of interest over the past 15 years. Indeed, the lackluster performances of typical coolants such as water, ethylene glycol and various oils have lead engineers to seek solutions for the increasing needs of heat transfer enhancement in current and future applications. For example, the reduction in size of high-performance electronic equipment (including micro processors) typically result in higher heat densities requiring more effective means of cooling. This can be accomplished by incorporating physical changes to the system (i.e. modifying the geometry of cooling apparatus) or by using alternate coolants. A review of literature on nanofluids will illustrate that the bulk of research on the subject initially consisted of determining nanofluid effective thermophysical properties such as thermal conductivity and viscosity (see for example Refs. [1,2] and [3]). More recently, attention has turned to their potential as coolants in practical engineering applications. Indeed, several studies on confined flow applications, including microchannels [4], radiator flat tubes [5] and finned tube heating units [6], have illustrated that nanofluids do have interesting heat transfer enhancement capabilities that would render them good candidates for usage in practical or industrial applications. Although several authors acknowledge that increases in viscosity will undoubtedly have effects on the overall performance of nanofluids in confined flow applications (for example, [7]), few have evaluated their overall performance. In some applications, their use could be somewhat compromised because of such increases in viscosity. Indeed, some authors have come to the conclusion that nanofluids are typically not favorable solutions when an overall energy balance analysis is considered, [8,9]. Furthermore, some studies have shown experimentally that the heat transfer of a SiC particle suspension in water is less efficient than using the base fluid alone, [10]. On the other hand, they found that the same SiC nanoparticles placed in an ethylene glycol/water mixture (50/50 volume ratio) will improve the cooling efficiency.

One other potentially interesting application of nanofluids recently considered is the confined impinging jet and/or radial flow cooling device. These types of flows are of considerable interest in the engineering community because of their numerous

* Corresponding author.
E-mail address: gilles.c.roy@umoncton.ca (G. Roy).

1290-0729/$ – see front matter © 2012 Elsevier Masson SAS. All rights reserved.
doi:10.1016/j.ijthermalsci.2012.03.009

Nomenclature

a	disk spacing, m
c_p	specific heat, J kg^{-1} K^{-1}
D	inlet diameter, $2R_{in}$, m
D_ω	cross-diffusion term for the SST $\kappa-\omega$ turbulence model
G_k	generation of κ
G_ω	generation of ω
h	heat transfer coefficient, W m^{-2} K^{-1}
k	thermal conductivity, W m^{-1} K^{-1}
k_b	Boltzmann's constant, 1.38066×10^{-23} J/K
l	inlet tube length, m
$\dot{m}$	mass flow rate, kg s^{-1}
M	molecular weight of the base fluid
N	Avogadro number, 6.022×10^{23} mol^{-1}
Nu	Nusselt number
p	pressure, Pa
PEC	Performance Evaluation Criterion
PP	pumping power, W
Pr	Prandtl number
Q	heat load, W
r	radial coordinate, m
R_{ext}	disk external radius, m
R_{in}	inlet radius, m
Re	Reynolds number (based on inlet)
Re_p	particle Reynolds number
Re_r	local Reynolds number
T	temperature, K
u_τ	friction velocity, m s^{-1}
v	velocity, m s^{-1}
$\overline{U}_{in}$	inlet average velocity, m s^{-1}
$\overline{U}_r$	mean velocity at radial position, m s^{-1}
$\dot{V}$	volumetric flow rate, m^3 s^{-1}
$\dot{W}$	pumping power, W
y	wall distance, m
$y+$	dimensionless wall distance, $y \cdot u_\tau/\nu$
Y_κ	dissipation of κ
Y_ω	dissipation of ω
z	axial coordinate, m

Greek symbols

α	thermal diffusivity, m^2 s^{-1}
κ	turbulent kinetic energy, m^2 s^{-2}
μ	fluid dynamic viscosity, Pa s
ν	fluid kinematic viscosity, m^2 s^{-1}
ω	specific dissipation rate, s^{-1}
φ	particle volume fraction, %
ρ	fluid density, kg m^{-3}

Subscripts

bf	with respect to base fluid
eff	effective property
f	with respect to fluid
in	with respect to inlet
m	mean value
nf	with respect to nanofluid
p	with respect to particles
r	with respect to radial coordinate
s	with respect to solid
w	with respect to wall
z	with respect to axial coordinate

applications requiring high localized cooling capabilities, including electronic component cooling equipment using liquids (see for example the works of Garimella and co-workers, [11] and [12] as well as those by Baydar and Ozmen [13]). Laminar flow cases of heat transfer and fluid flow of nanofluids in these types of applications have been considered recently, [14–18]. In general, results presented by these authors indicate that nanofluids have the potential of becoming interesting alternatives to traditional liquids such as water (i.e., increases in heat transfer coefficients and Nusselt's numbers, etc.). In particular, results presented by Feng and Kleinstreuer, [17], seem to indicate that nanofluids reduce the cooling system's total entropy generation rate with minimal effects on required pumping power. Also of interest, numerical results presented by Yang and Lai [16,18], show that for fixed values of pumping power, nanofluids do not always offer improved heat transfer rates. They have also found that the heat transfer enhancement of nanofluids increases with heat flux. Results presented by these authors were validated with the experimental data presented by Gherasim et al., [15]. On a related note, Manca et al., [19], have presented a numerical study of the case of a confined slot impinging jet with nanofluids. As in the radial flow cases previously discussed, they have found that for an increase in particle concentrations, nanofluids produce related increases in fluid bulk temperature, in Nusselt number, in heat transfer coefficient and in pumping power.

It therefore seems clear that further research is required in order to fully understand the behavior of nanofluids as well as to quantify the extent of their potential use in engineering applications. This includes confined impinging jet and radial flow cooling systems. To our knowledge, turbulent confined radial flows and heat transfer of nanofluids have yet to be considered in literature. Furthermore, the controversy regarding the efficacy of nanofluids will be addressed by considering potentially limiting factors such as related increases in pumping power. The Performance Evaluation Criterion proposed by Ferrouillat et al., [9] will also be considered in this paper.

2. Mathematical modeling and numerical approach

2.1. Problem geometrical configuration

The configuration modeled in this paper is similar to the geometry considered in the study by Gherasim et al. [20], Fig. 1. The

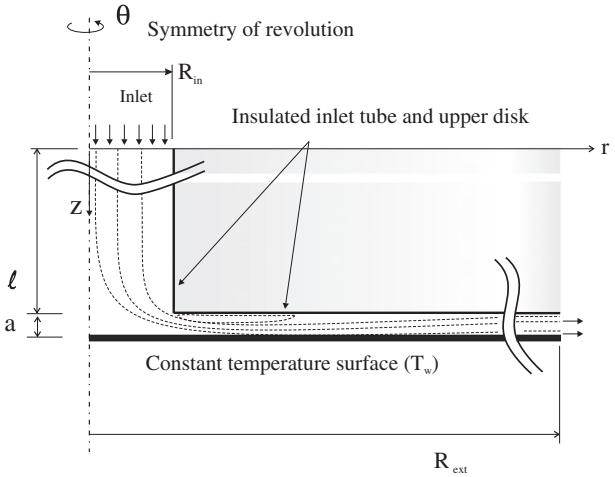

Fig. 1. Considered geometry for numerical model (not to scale).

turbulent flow and heat transfer of the considered nanofluid flowing inside the resulting radial channel between a heated disk and a large frontal area nozzle (i.e. second, parallel disk) is considered. Coolant flow enters through an inlet orifice of radius $R_{in} = 3.97$ mm ($D = 7.94$ mm), travels downstream through a radial channel to the outer radius $R_{ext} = 12.75$ cm. The disks are separated by a gap "a" which can be varied (typically between 1 and 5 mm). An inlet tube of $l = 32$ cm is considered in all cases in order to permit fully developed flow as well as to minimize possible inlet boundary condition influences in the region of interest.

2.2. Governing equations

The type of flow considered in this present paper can be characterized by a set of coupled partial derivative equations. Indeed, considering the single-phase fluid assumption previously discussed and by neglecting compression work, the typical governing equations (i.e. Navier–Stokes equations) for single phase fluid flow can be used. The resulting governing equations are therefore the continuity equation, the conservation of momentum equations and the conservation of energy equation. For turbulent flows of the type considered in this present paper, the Reynolds averaged Navier–Stokes (RANS) equations are commonly used to numerically solve the flow and thermal fields. In order to obtain the RANS equations, the instantaneous values are decomposed into average and fluctuation values. Various turbulence models have been developed over time. As will be discussed in more detail in Section 2.6.2, the shear stress transport (SST) $\kappa - \omega$ turbulence model will be used in this present work. This model requires two additional equations, namely the turbulent kinetic energy and the energy dissipation rate equations. The single-phase governing equations in cylindrical coordinates can now be expressed as follows (see for example Ref. [21]). Note that all symbols referring to the flow and thermal fields dependent variables are time-averaged values of these variables.

- conservation of mass

$$\frac{1}{r}\frac{\partial(rv_r)}{\partial r} + \frac{\partial v_z}{\partial z} = 0 \tag{1}$$

- conservation of momentum

$$\frac{1}{r}v_r\frac{\partial(rv_r)}{\partial r} + v_z\frac{\partial v_r}{\partial z} = -\frac{1}{\rho}\frac{\partial p}{\partial r} + (\nu + \nu_t)\left[\frac{1}{r}\frac{\partial}{\partial r}\left(\frac{\partial(rv_r)}{\partial r}\right) + \frac{\partial}{\partial z}\left(\frac{\partial v_z}{\partial z}\right)\right] \tag{2}$$

$$v_z\frac{\partial v_z}{\partial z} + \frac{1}{r}v_r\frac{\partial(rv_z)}{\partial r} = -\frac{1}{\rho}\frac{\partial p}{\partial z} + (\nu + \nu_t)\left[\frac{1}{r}\frac{\partial}{\partial r}\left(\frac{\partial(rv_r)}{\partial r}\right) + \frac{\partial}{\partial z}\left(\frac{\partial v_z}{\partial z}\right) - \frac{v_r}{r^2}\right] \tag{3}$$

- conservation of energy

$$\frac{1}{r}\frac{\partial(v_rT)}{\partial r} + \frac{\partial(v_zT)}{\partial z} = \frac{1}{r}\frac{\partial}{\partial r}\left[r\alpha_{eff}\frac{\partial T}{\partial r}\right] + \frac{\partial}{\partial_z}\left[\alpha_{eff}\frac{\partial T}{\partial_z}\right] \tag{4}$$

- turbulent kinetic energy

$$\frac{1}{r}v_r\frac{\partial(r\kappa)}{\partial r} + v_z\frac{\partial \kappa}{\partial z} = \left(\nu + \frac{\nu_t}{\sigma_\kappa}\right)\left[\frac{1}{r}\frac{\partial}{\partial r}\left(\frac{\partial(r\kappa)}{\partial r}\right) + \frac{\partial}{\partial z}\left(\frac{\partial \kappa}{\partial z}\right)\right] + G_\kappa - Y_\kappa \tag{5}$$

- energy dissipation rate

$$\frac{1}{r}v_r\frac{\partial(r\omega)}{\partial r} + v_r\frac{\partial \omega}{\partial z} = \left(\nu + \frac{\nu_t}{\sigma_\omega}\right)\left[\frac{1}{r}\frac{\partial}{\partial r}\left(\frac{\partial(r\omega)}{\partial r}\right) + \frac{\partial}{\partial z}\left(\frac{\partial \omega}{\partial z}\right)\right] + G_\omega - Y_\omega + D_\omega \tag{6}$$

where, in Equations (5) and (6), G_κ and Y_κ are respectively the turbulent kinetic energy and the dissipation of turbulence kinetic energy and G_ω and Y_ω are respectively the generation of ω and the dissipation of ω due to turbulence. The term D_ω represents the cross-diffusion term for the SST $\kappa - \omega$ turbulence model. These quantities are defined and appropriately developed in the references [22,23].

2.3. Boundary conditions

The equation system described in the previous section is a set of non-linear coupled equations requiring the use of an appropriate set of boundary conditions. The following were used (see Fig. 1):

- at the tube inlet section ($z = 0$ and $0 \le r \le R_{in}$), a uniform axial velocity and temperature profile as well as turbulence intensity and hydraulic diameter are specified;
- on the inlet tube wall ($r = R_{in}$ and $0 \le z \le l$) and the upper disk ($z = l$ and $R_{in} \le r \le R_{ext}$), the no-slip condition and insulated wall are specified;
- on the vertical axis passing through the center of the disks ($r = 0$ and $0 \le z \le l + a$), conditions of symmetry of revolution are used;
- on the impinged surface ($z = l + a$ and $0 \le r \le R_{ext}$), a constant disk wall temperature and the no-slip condition are imposed;
- At the domain outlet section ($r = R_{ext}$ and $l \le z \le l + a$), ambient conditions prevail (i.e. pressure).

2.4. Thermal and physical properties of nanofluids

As mentioned in the previous section, the single phase approach will be used to model nanofluid behavior inside the considered cooling system. To accomplish this, nanofluid effective properties are required. For all considered properties (i.e. density, specific heat, dynamic viscosity and thermal conductivity), the base fluid values (i.e. water) are considered to be temperature dependant and are calculated from correlations obtained from tabulated data from the ASHRAE Handbook of Fundamentals, [24].

2.4.1. Nanoparticle properties

Three water-based nanofluids containing Al_2O_3, CuO and TiO_2 nanoparticles of various concentrations (or volume fractions, ϕ) will be considered In order to determine the temperature dependant nanofluid effective properties, nanoparticle physical properties must be specified. The data used in this present paper is presented, with appropriate references, in Table 1. The data presented in Table 1 will be used in Eqs. (7)–(13) for the calculation of nanofluid effective properties (see following subsections).

2.4.2. Density

Nanofluid density is obtained by measuring the volume and weight of the mixture. The particle volume fraction ϕ can be estimated knowing the densities of both constituents, Eq. (7):

$$\rho_{nf} = \varphi\cdot\rho_p + (1 - \varphi)\cdot\rho_{bf} \tag{7}$$

By rearranging equation (7), one can therefore determine the volume fraction "ϕ" of the mixture, Eq. (8).

$$\varphi = \frac{\rho_{nf} - \rho_{bf}}{\rho_p - \rho_{bf}} \tag{8}$$

2.4.3. Specific heat

Thus far, only a few sets of experimental data on nanofluid effective specific heat can be found in literature, [7,29,30]. As

discussed in Gherasim et al., [15], an approach based on the heat capacity concept (thermal equilibrium), [31–34] seems the most appropriate.

$$(\rho c_p)_{nf} = (1-\varphi)\cdot(\rho c_p)_{bf} + \varphi\cdot(\rho c_p)_{p} \quad (9)$$

where the specific heat and density terms in $(\rho c_p)_{bf}$ are temperature dependant values for water.

2.4.4. Thermal conductivity

Over the past decade, several authors have investigated nanofluid effective properties, including thermal conductivity. These included experimental evaluation (see for example Ref. [35]) as well as various correlations (amongst others, [36,37]). In this present paper, the correlation recently developed by Corcione [38] is used to approximate the nanofluid effective thermal conductivity, Eq. (10). This correlation is based on a comprehensive set of experimental data by various authors.

$$\frac{k_{eff}}{k_{bf}} = 1 + 4.4\mathrm{Re}_p^{0.4}\mathrm{Pr}_{bf}^{0.66}\left(\frac{T}{T_{fr}}\right)^{10}\left(\frac{k_s}{k_{bf}}\right)^{0.03}\varphi^{0.66} \quad (10)$$

where, T_{fr} is the freezing point of the base liquid, Re_p is the nanoparticle Reynolds number, Eq. (11), and Pr_{bf} is the base fluid Prandtl number, Eq. (12):

$$\mathrm{Re}_p = \frac{2\rho_{bf}k_b T}{\pi\mu_{bf}^2 d_p} \quad (11)$$

where k_b is the Boltzmann's constant ($k_b = 1.38066\times10^{-23}$ J/K).

$$\mathrm{Pr}_{bf} = \frac{c_{p_{bf}}\cdot\mu_{bf}}{k_{bf}} \quad (12)$$

All base fluid properties in Eqs. (11) and (12) are temperature dependant.

2.4.5. Dynamic viscosity

As with nanofluid effective thermal conductivity, several authors have investigated rheological properties of nanofluids (these include Refs. [39,40]). For the purposes of this paper, the correlation recently developed by Corcione, [38], is used to approximate the nanofluid effective viscosity, Eq. (13). This correlation is also based on a comprehensive set of experimental data by various authors.

$$\frac{\mu_{eff}}{\mu_f} = \frac{1}{1-34.87\left(\frac{d_p}{d_f}\right)^{-0.3}\varphi^{1.03}} \quad (13)$$

where, as stated in Ref. [38], d_f is the equivalent diameter of a base fluid molecule, Eq. (14):

$$d_f = 0.1\left[\frac{6M}{N\pi\rho_{f0}}\right]^{\frac{1}{3}} \quad (14)$$

where in Eq. (14) M and N are respectively the molecular weight of the base fluid and the Avogadro number (6.022×10^{23} mol^{-1}) and ρ_{f0} is the mass density of the base fluid calculated at $T_0 = 293$ K.

Table 1
Nanoparticle properties used in numerical model.

	Nanoparticle type		
	Al_2O_3[a]	CuO[b]	TiO_2[c]
Particle diameter (nm)	47	29	27
ρ (kg/m^3)	3880	6500	4175
k (W/m K)	36	32.6	8.4
c_p (J/kg K)	773	530	692

[a] Data from Ref. [25].
[b] Data from Refs. [26], [27].
[c] Data from Ref. [28].

2.5. Governing dimensionless parameters

The considered problem can be characterized by a set of dimensionless parameters, namely the inlet Reynolds number, Re_{in}, the Nusselt number, Nu, various aspect ratios and the particle volume fraction ϕ. The Reynolds and Nusselt numbers are defined as follows, Eqss. (15) and (16):

$$\mathrm{Re} = \frac{\overline{U}_{in}\cdot D\cdot\rho_{nf}}{\mu_{nf}} \quad (15)$$

$$\mathrm{Nu} = \frac{h\cdot D}{k_{nf}} \quad (16)$$

2.6. Numerical method, validation and grid sensitivity testing

2.6.1. Numerical approach

The finite volume method was used to solve the set of governing equations (Fluent 6.3.26). As this method is well-known, only a few general comments will be made here. More details can be obtained in, for example, [41] or [42]. The classical staggered grid finite volume approach was used throughout this paper. The SIMPLEC algorithm with the TriDiagonal Matrix Algorithm (TDMA) were used to integrate and solve the discretized governing equations over each control volume.

2.6.2. Turbulence modeling and validation

A review of literature shows that a variety of turbulence models have been used in the past for cases considering radial flows between disks as well as confined impinging jets. These include the standard $\kappa-\varepsilon$ model (see for example Ref. [13]) as well as the v^2-f (non-linear eddy-viscosity) (see Ref. [43]) and the $\kappa-\omega$ SST models (see Ref. [44]). The $\kappa-\omega$ SST model ("Shear Stress Transport") is a relatively recent, RANS-based, two-equation eddy-viscosity model developed by Menter ([22]). It has been shown to be quite adequate for applications with separating flows. The model essentially combines the benefits of being usable as a low Reynolds turbulence model (i.e. modeling in the viscous sub-layer) as well as having a $\kappa-\varepsilon$ behavior in the free-stream. To our knowledge, no experimental results have thus far surfaced for the case of turbulent radial flow and heat transfer of a nanofluid in a confined impinging jet application. The majority of work conducted so far on radial flow and/or confined impinging jets have considered air or water as coolants. Results obtained when using this model for the particular geometry of interest are therefore compared with various experimental data and other turbulence models in Fig. 2 using air as the working fluid. In Fig. 2 (a), Nusselt number results obtained with the $\kappa-\omega$, $\kappa-\omega$ SST, $\kappa-\varepsilon$ and v^2-f models are considered and compared with experimental data obtained by Gao and Ewing [45]. In general, the $\kappa-\omega$ SST model seems to replicate the behavior quite well. Indeed, the first crest is found at approximately the same location ($r/D \approx 0.5$) although numerical simulations yield Nusselt values approximately 10% higher. Further downstream, both $\kappa-\omega$ SST and the v^2-f models capture the second crest, although at different radii. When compared to experimental results, the $\kappa-\omega$ SST model seems to replicate the behavior more closely. The

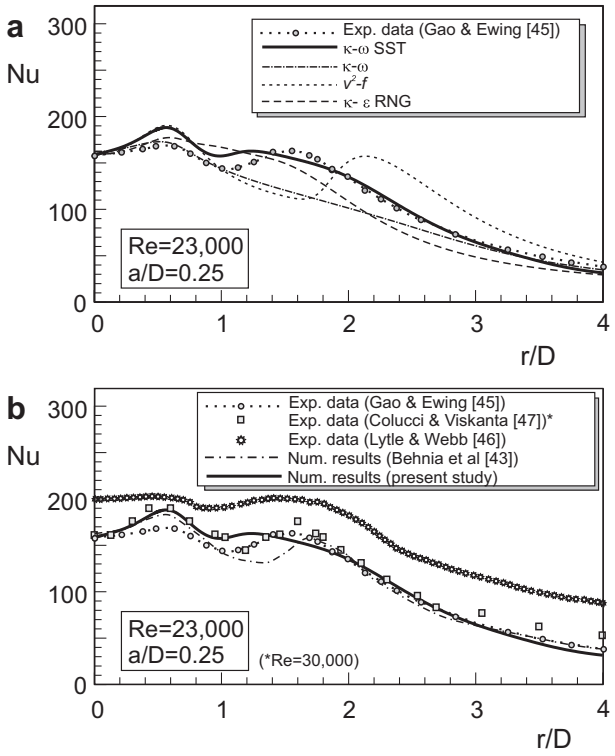

Fig. 2. Impinged surface local Nusselt number comparisons with results obtained by various authors.

remaining two models (i.e. $\kappa-\omega$ and $\kappa-\varepsilon$) seem inadequate for this application. This is to be expected as the type of geometry considered is well known for having separating flows. In Fig. 2 (b), results obtained with the $\kappa-\omega$ SST model are compared to three sets of experimental data ([46,47] and the aforementioned Gao and Ewing data [45]) as well as with results obtained numerically using the v^2-f model [43]. A certain amount of scatter is found between experimental results obtained by the various authors and the results obtained in this present study using the $\kappa-\omega$ SST model falls within the available experimental data. The experimental work by Gao and Ewing [45] also presented wall pressure distributions, a comparison with numerical results in this study is thus presented in Fig. 3. A maximum difference of approximately 10% is found between the numerical results. On a final note with respect to turbulence modeling, for a geometrically similar case (i.e. the radial airflow diffuser), Colaciti et al. [44] also concluded that the $\kappa-\omega$ SST model was a good choice.

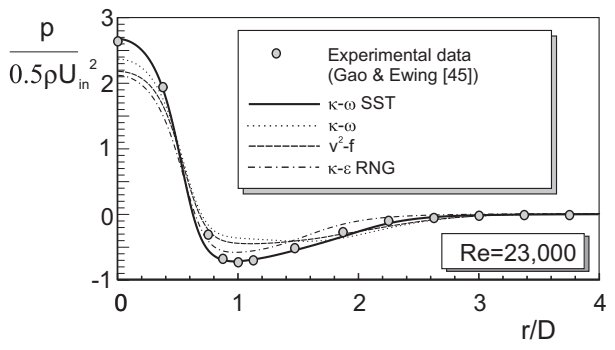

Fig. 3. Impinged surface wall pressure distribution comparisons with experimental data by Gao and Ewing [40].

Although the domain extends to $r/D = 16$, results are presented in the region of interest, $r/D = 4$. Again, the maximum difference between numerical results and experimental data is estimated at 10%.

2.6.3. Grid sensitivity testing

In order to insure grid-independent solutions, several grids have been thoroughly tested. In all cases, the $\kappa-\omega$ SST model was used. A grid of 160 × 1000 in the channel between disks was finally chosen (280,000 nodes in total). The grid points are highly packed near the radial channel inlet as well as on all walls. Of interest, a typical case with this number of nodes takes approximately 16 h to converge whereas a case with 240 × 1500, yielding practically identical results, took more than 100 h. Furthermore, $y+$ values were inferior to unity in all considered cases.

2.6.4. Convergence criterion

The convergence criterion for all computations presented in this paper were based on the residuals that result from the integration of the conservation equations (see Section 2.2) over the finite control-volumes. During the iterative process, these residuals were monitored. Converged solutions were considered achieved when the residuals were found to be inferior to 10^{-8}.

3. Results and discussion

As we are essentially interested in evaluating the performance of various types of nanofluids in a radial flow cooling system, multiple cases were considered. Unless otherwise specified, the considered cases had the following parameters:

- Uniform inferior disk temperature: $T_{wall} = 323$ K
- Inlet Reynolds number range: $100 \leq Re \leq 50{,}000$
- Particle loadings: $\phi = 0$, 2, 4 and 6%
- Geometrical quantities: $D = 7.94$ mm, $R_{ext} = 12.75$ cm, $a = 2$ mm
- Non dimensional geometrical quantities: $a/D = 0.252$ $R_{ext}/D = 16$
- Water-based nanofluid types: Al_2O_3, CuO and TiO_2

Details on particle sizes, etc. were given in Table 1. Most presented cases are for Al_2O_3 type nanofluids, however, the general behaviors were found to be essentially the same for the other two considered particle types. Comparisons between the three types will be illustrated and discussed in Section 3.4.

3.1. Hydrodynamic and thermal analysis of flow field

3.1.1. General behavior

As previously stated, fluid flow between two parallel disks has been a subject of considerable interest of the past half-century as applications of this type of flows are numerous, especially for localized cooling situations. In order to get an overall appreciation of the hydrodynamic and thermal fields, Fig. 4 illustrates the flow contour lines, the pressure, temperature and kinetic energy fields as well as wall pressure distributions and Nusselt numbers as functions of r/D for a typical case ($Re = 25{,}000$, $\phi = 4\%$, Al_2O_3 nanofluid). Although the considered domain extends to $r/D = 16$, the area or particular interest covers the region between $0 \leq r/D \leq 4$. As could be expected, a flow recirculation zone is found on the surface of the nozzle (i.e. upper disk) for a region extending from the inlet lip ($r/D = 0.5$) to approximately $r/D = 3.0$. This essentially represents a *vena-contracta* effect. Associated with this recirculation area is a considerable flow acceleration near the surface of the impinged disk represented by a tightening of the

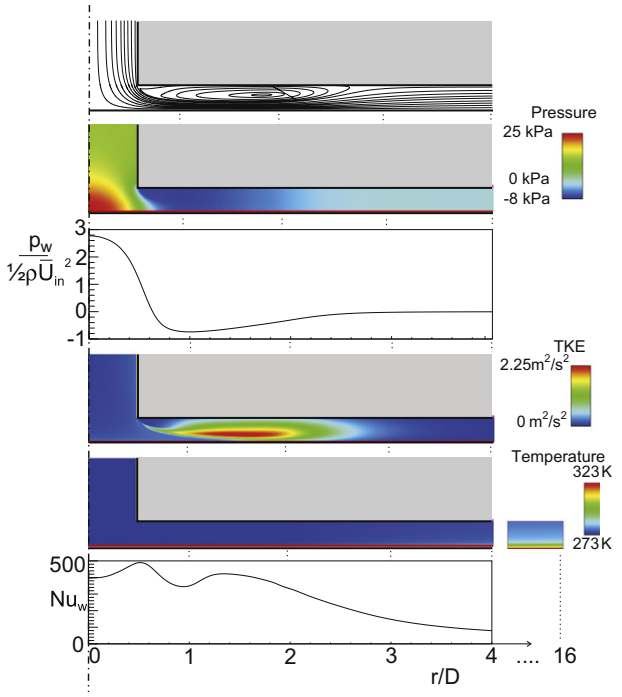

Fig. 4. Hydrodynamic and thermal field for a typical case.

contour lines and the corresponding decrease in pressure. Indeed, a subatmospheric pressure area is found for the entire region covered by the recirculation zone. This particular region is also where the kinetic turbulent intensity is the most important in the flow field (this will be discussed in the next section). With respect to the temperature field, the fluid's temperature gradually increases with radius. Logically, the region near the heated disk's surface is heated initially with the temperature gradually increasing in the axial direction further downstream. As the temperature generally does not increase much in the region near the injection inlet ($r/D \leq 4$), temperature floods are shown for the region near the periphery (i.e. $15.5 \leq r/D \leq 16$). Finally, the bottom part of Fig. 4 illustrates the local Nusselt number distribution. The general behavior is essentially the same as found by other authors using typical coolants (illustrated in Fig. 2). Generally, the increases in Nusselt numbers can be associated with the local acceleration of the fluid. Indeed, the first peak is located at the lip of the injection nozzle at the entrance of the radial flow section whereas the second peak is located near the maximum flow restriction area (at approximately $r/D = 1.5$ – also represented by the tightening of flow contour lines).

3.1.2. Turbulence decay and relaminarisation

One particularly interesting aspect of turbulent radial flow is turbulence decay and flow relaminarisation. Indeed, as the flow section increases with radius, the corresponding flow velocity decreases thus permitting, with favorable flow conditions, a transition from fully turbulent flow conditions to laminar flow. Particularly of interest are the findings of [48] and [49]. Moller defined a local Reynolds number based on the radius of the parallel disks, Eq. (17):

$$\mathrm{Re}_{r,\mathrm{Moller}} = \frac{\rho \cdot \overline{U}_{in} \cdot R_{in}^2}{\mu \cdot r} = \frac{\mathrm{Re} \cdot R_{in}}{2r} \tag{17}$$

In the case of [49], the local Reynolds number was defined as Eq. (18):

$$\mathrm{Re}_{r,TP} = \frac{2 \cdot \overline{U}_r \cdot h}{\nu} \tag{18}$$

where, in this equation, $h = 0.5a$. With a few manipulations, we find Eq. (19):

$$\mathrm{Re}_{r,TP} = \frac{\mathrm{Re}_{r,\mathrm{Moller}}}{2} \tag{19}$$

In Moller's case, analysis from results seem to indicate that flow relaminarisation occurred in the vicinity of $\mathrm{Re}_r = 2000$. Tabatabai and Pollard [49] also presented an interesting and comprehensive study of turbulent radial flow between parallel disks. They found that relaminarization is a rather gradual process and at low local Reynolds numbers, the turbulence decays and eventually quasi-laminar boundary layer gradually replaces the viscous sub-layer. In this present paper, we will use the following Eq. (20) which is essentially based on Moller's definition:

$$\mathrm{Re}_r = \frac{\mathrm{Re} \cdot R_{in}}{2r} \tag{20}$$

Fig. 5 (a) and (b) illustrates the kinetic turbulent energy as a function of radial position. Fig. 5 (a) presents for a typical particle loading of 2% the kinetic turbulent energy for three different axial positions within the radial channel (i.e. $a/3$, $a/2$ and $2a/3$). As can be seen, the kinetic turbulent energy "k" is more important near the heated surface (i.e. impacted disk, $z = l + 2a/3$). As was noticed in Fig. 4, this area is represented by flow acceleration as the fluid leaves the nozzle (axial flow) and is redirected radially. The kinetic

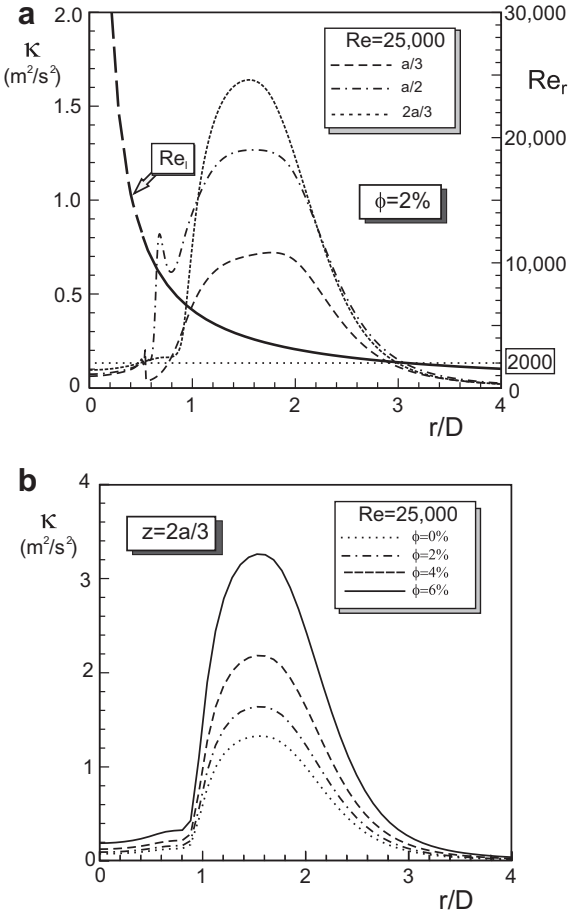

Fig. 5. Turbulent kinetic energy distributions and local Reynolds number.

turbulent energy is less pronounced near the nozzle surface (i.e. upper disk) as this region is represented by a recirculation area. Of interest, the local Reynolds number, as defined by Eq. (20) is plotted on the same figure. As the flow channel area increases with radius, the local Reynolds number decreases. Furthermore, after reaching maximum values near $r/D = 1.8$, the kinetic turbulent energy also decreases gradually with the radius. At approximately $r/D = 3$, the local Reynolds value decreases to a value of 2000 and the turbulent kinetic energy decreases rapidly as well. One can see that for approximately $r/D > 4$, "k" tends asymptotically to zero. This general behavior seems consistent with what was found by [48] and [49].

In Fig. 5 (b), the kinetic turbulent energy is plotted at $z = l + 2a/3$ for various particle loadings for Re = 25,000. The influence of an increase in coolant viscosity is clearly discernable. Indeed, for a given Re, "k" increases with ϕ.

3.2. Parametric study of heat transfer enhancement

Heat transfer enhancement of nanofluids is assessed considering the influence of particle loadings and Reynolds number on Nusselt number, Fig. 6. The average Nusselt number used for comparisons are surfaced-averaged values (for details, see Ref. [20]). As can be seen, both Reynolds number and particle loading have positive impacts on the average Nusselt number. For example, for Re = 50,000, the use of a 6% particle loading nanofluid will provide an increase of approximately 15% in Nusselt number when compared to the value obtained with water. This is consistent with what is typically found in current literature.

3.3. Nanofluid heat transfer enhancement efficacy

A quick review of literature on nanofluids will generally show that they have the potential to provide, in quite a few cases, considerable heat transfer benefits. However, their overall performance as heat transfer mediums has rarely been discussed. As one could expect, the addition of nanoparticles into a base fluid will not only enhance heat transfer but will also increase shear stresses and pressure losses. This is an important factor to consider when choosing an appropriate coolant for a specific application. Therefore, an attempt to quantify the benefits versus drawbacks (or efficacy) of the use of nanofluids as coolants in radial flow cooling systems is presented by considering such factors as pumping power.

Pumping power is defined by Eq. (21), see for example Refs. [50,51]:

$$\mathrm{PP} = \dot{W} = \dot{V} \cdot \Delta p_t = \frac{\dot{m} \cdot \Delta p_t}{\rho} \tag{21}$$

where Δp_t is the total pressure difference between the inlet and outlet sections of the computational domain.

In Fig. 7, the required pumping power is presented in function of Reynolds number. The addition of nanoparticles to the base coolant will undoubtedly have major consequences on pumping power. Indeed, for Re = 50,000, a 4.5 fold increase in pumping power is found when using a 6% particle volume fraction nanofluid when compared to water.

Although Figs. 6 and 7 provide interesting information on heat transfer enhancement and pumping power behaviors of nanofluids, their overall performance (or efficacy) is somewhat more difficult to assess. An approach that can be considered in evaluating various coolants would be to consider the required pumping power for a given heat duty, Fig. 8. It seems clear that, at least for the geometric configuration under consideration, water requires less pumping power to evacuate a certain heat load than all of the nanofluids evaluated. Indeed, for a given heat duty, an increase in particle volume fraction will require more pumping power. For example, a 6% nanofluid will require approximately 2.5 times more pumping power than pure water to evacuate an 8 kW heat load. One can also note here that the differences found would most certainly be amplified if the whole pumping circuit where considered (i.e. including all piping, valves, heat exchangers, etc…). Similar conclusions were made by Pantzali and co-workers in their studies with CuO based nanofluids in plate heat exchangers, [8].

Another criterion that can be used to evaluate nanofluid overall energetic performance is the *Performance Evaluation Criterion* (or *PEC*), [9]. This criterion is based on the ratio of heat transferred to the required pumping power in the test section, Eq. (22):

$$\mathrm{PEC} = \frac{\dot{m} \cdot c_p \cdot \Delta T}{\dot{V} \cdot \Delta p_t} \tag{22}$$

where ΔT and Δp_t are respectively the temperature and pressure differences between the outlet and inlet sections. Results for PEC as

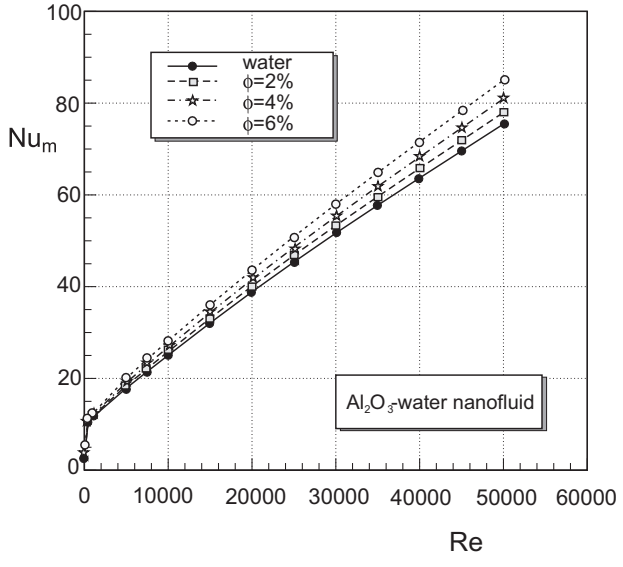

Fig. 6. Average Nusselt number in function of Reynolds number.

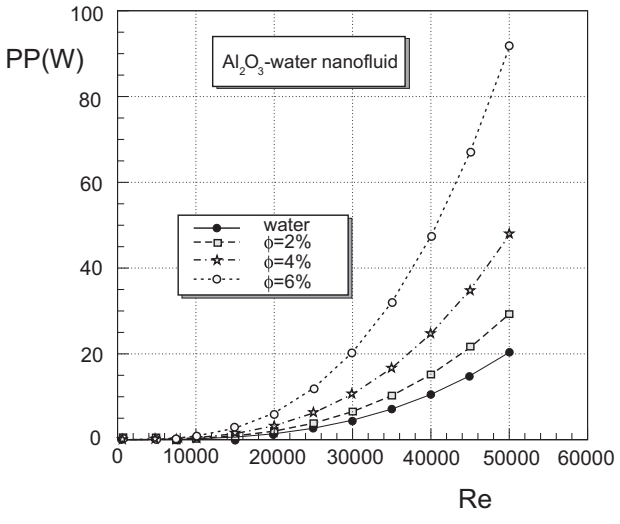

Fig. 7. Pumping power in function of Reynolds number.

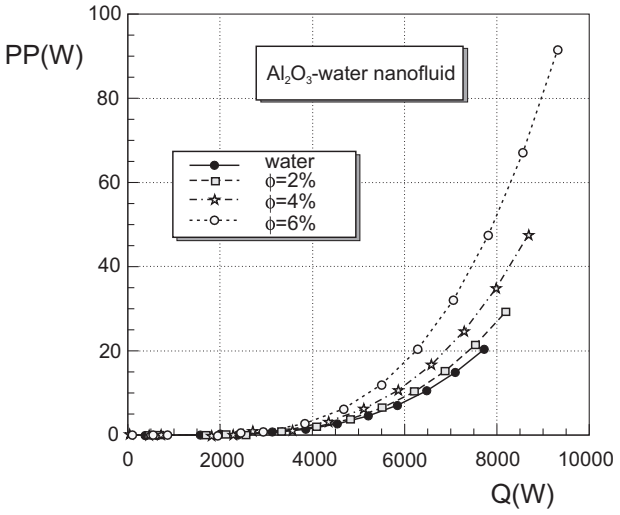

Fig. 8. Pumping power required to handle a given heat load.

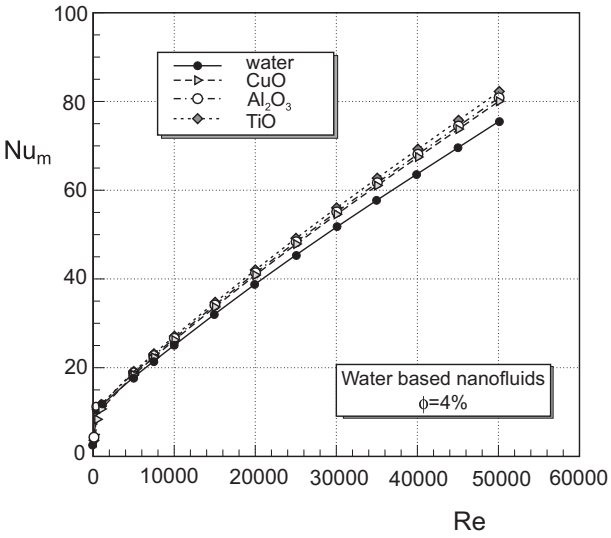

Fig. 10. Nanofluid type mean Nusselt number comparisons.

a function of Reynolds number for various particle loading are presented in Fig. 9. For the purposes of having results for a larger Reynolds number range, a few laminar cases are added for $Re \leq 1000$. Again, the same conclusions are reached. Indeed, one can see that pure water has a higher PEC than any of the considered particle loadings for any given Reynolds number, laminar or turbulent. The same overall assessment was reached by [9] for a SiO_2 nanofluid in a horizontal tube.

3.4. Nanofluid type comparisons

Results presented in this paper thus far are typically for Al_2O_3 water-based nanofluids. It should be noted however that the same general behaviors were found for all three types of nanofluids (CuO and TiO being the other two types). In this section, the three considered nanofluids will be compared. Fig. 10 illustrates Nusselt number comparisons for a same particle loading (i.e. $\phi = 4\%$). Although small differences are found, results for all three types of nanofluids are quite similar, with the TiO nanofluid yielding slightly higher Nu_m values in the entire Re range.

Comparisons for the *Performance Evaluation Criterion* are presented in Fig. 11. Again, results for the three types of nanofluids are essentially the same. This time, the Al_2O_3 nanofluid seems to have slightly higher *PEC* values compared to the other two types. For all the considered cases, pure water is the most "energy efficient" coolant.

3.5. General remarks on nanofluid performance

Results presented in this section show that heat transfer enhancement is found for all types of nanofluids considered. However, when energy-based performance comparisons are made, pure water was the most efficient coolant of all those considered. This is not to say that nanofluids do not have potential roles in specialized cooling situations, however, they do not seem to provide the anticipated overall benefits, at least in this application, that researchers had originally hoped for. These results are however consistent with several other recently published works on

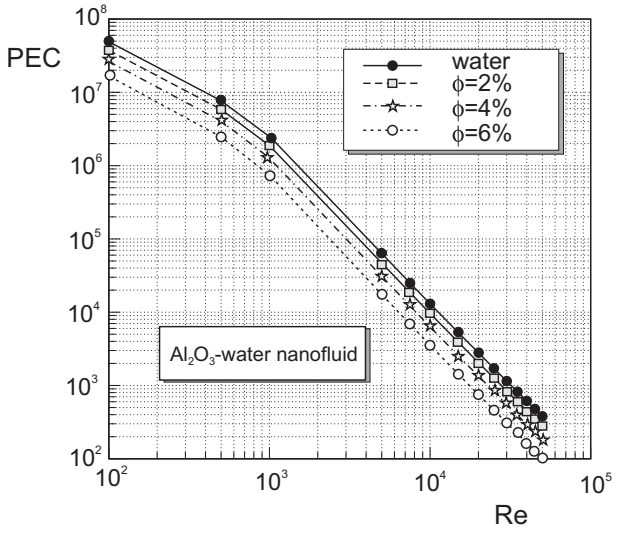

Fig. 9. Performance Evaluation Criterion (PEC) as a function of Reynolds number.

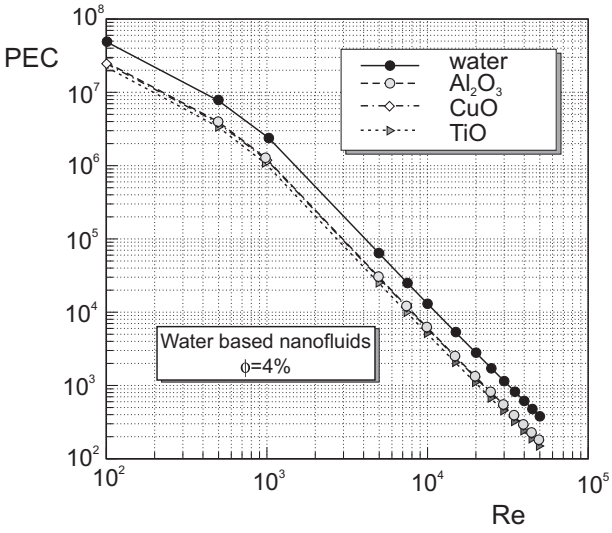

Fig. 11. Nanofluid type PEC comparisons.

nanofluid heat transfer applications, see for example Refs. [8] (plate heat exchangers) and [9] (horizontal tube flow). Essentially, a reduction in nanofluid effective viscosity would be required to increase their overall efficacy. More research into nanofluid manufacturing techniques (including further particle size reduction, suspension agents, etc…) could possibly render nanofluids more attractive for practical applications.

4. Conclusion

A numerical investigation on water-based nanofluids inside a radial turbulent flow cooling system was presented in this paper. Results indicated that the $\kappa - \omega$ SST turbulence model is a good choice for the numerical turbulence modeling of this type of geometrical configuration. As a single-phase approach was considered in this paper, correlations found in recent literature were used to compute the nanofluid effective properties. Although heat transfer enhancement was found for all the types of nanofluids considered, their overall performance seems to indicate that their usage in practical applications may not be as beneficial as originally hoped for due to the corresponding increases in pumping power.

Acknowledgments

The authors of this paper wish to thank the New Brunswick Innovation Fund (NBIF/FINB) and the Université de Moncton's Faculty of graduate studies (FESR) for financial support to this project.

References

[1] S. Murshed, K. Leong, C. Yang, Thermophysical and electrokinetic properties of nanofluids – a critical review, Applied Thermal Engineering 28 (2008) 2109–2125.
[2] P. Keblinski, R. Prasher, J. Eapen, Thermal conductance of nanofluids: is the controversy over? Journal of Nanoparticle Research 10 (7) (2008) 1089–1097.
[3] V. Trisaksri, S. Wongwises, Critical review of heat transfer characteristics of nanofluids, Renewable and Sustainable Energy Reviews 11 (3) (2007) 512–523.
[4] J. Li, C. Kleinstreuer, Thermal performance of nanofluid flow in microchannels, International Journal of Heat and Fluid Flow 29 (2008) 1221–1232.
[5] R. Vajjha, D.K. Das, P.K. Namburu, Numerical study of fluid dynamic and heat transfer performance of Al_2O_3 and CuO nanofluids in the flat tubes of a radiator, International Journal of Heat and Fluid Flow 31 (2010) 613–621.
[6] R. Strandberg, D.K. Das, Finned tube performance evaluation with nanofluids and conventional heat transfer fluids, International Journal of Thermal Sciences 49 (2010) 580–588.
[7] P. Namburu, D. Kulkarni, A. Dandekar, D. Das, Experimental investigation of viscosity and specific heat of silicon dioxide nanofluids, Micro & Nano Letters 2 (3) (2007) 67–71.
[8] M. Pantzali, A. Mouza, S. Paras, Investigating the efficacy of nanofluids as coolants in plate heat exchangers (PHE), Chemical Engineering Science 64 (2009) 3290–3300.
[9] S. Ferrouillat, A. Bontemps, J.-P. Ribeiro, J.-A. Gruss, O. Soriano, Hydraulic and heat transfer study of SiO_2/water nanofluids in horizontal tubes with imposed wall temperature boundary conditions, International Journal of Heat and Fluid Flow 32 (2011) 424–439.
[10] E.V. Timofeeva, W. Yu, D.M. France, D. Singh, J.L. Routbort, Base fluid and temperature effects on the heat transfer characteristics of SiC in ethylene glycol/H_2O and H_2O nanofluids, Journal of Applied Physics 109 (014914) (2011) 1–5.
[11] S.V. Garimella, R.A. Rice, Confined and submerged liquid jet impingement heat transfer, Journal of Heat Transfer 117 (117) (1995) 871–877.
[12] S.V. Garimella, B. Nenaydykh, Nozzle-geometry effects in liquid jet impingement heat transfer, International Journal of Heat and Mass Transfer 39 (14) (1996) 2915–2923.
[13] E. Baydar, Y. Ozmen, An experimental and numerical investigation on a confined impinging air jet at high Reynolds numbers, Applied Thermal Engineering 25 (2005) 409–421.
[14] S.E.B. Maiga, S.J. Palm, C.T. Nguyen, G. Roy, N. Galanis, Heat transfer enhancement by using nanofluids in forced convection flows, International Journal of Heat and Fluid Flow 26 (2005) 530–546.
[15] I. Gherasim, G. Roy, C.T. Nguyen, D. Vo-Ngoc, Experimental investigation of nanofluids in confined laminar radial flow, International Journal of Thermal Sciences 48 (2009) 1486–1493.
[16] Y.-T. Yang, F.-H. Lai, Numerical study of heat transfer enhancement with the use of nanofluids in a radial flow cooling system, International Journal of Heat and Mass Transfer 53 (2010) 5895–5904.
[17] Y. Feng, C. Kleinstreuer, Nanofluid convective heat transfer in a parallel-disk system, International Journal of Heat and Mass Transfer 53 (2010) 4619–4628.
[18] Y.-T. Yang, F.-H. Lai, Numerical investigation of cooling performance with the use of Al_2O_3/water nanofluids in a radial flow system, International Journal of Thermal Sciences 50 (2011) 61–72.
[19] O. Manca, P. Mesolella, S. Nardini, D. Ricci, Numerical study of a confined slot impinging jet with nanofluids, Nanoscale Research Letter 6 (188) (2011) 1–16.
[20] I. Gherasim, G. Roy, C.T. Nguyen, D. Vo-Ngoc, Heat transfer enhancement and pumping power in confined radial flows using nanoparticle suspensions (nanofluids), International Journal of Thermal Sciences 50 (2011) 368–377.
[21] A.A. Ganguli, A.B. Pandit, J.B. Joshi, P.K. Vijayan, Hydrodynamic and heat transfer characteristics of a centrally heated cylindrical enclosure: CFD simulations and experimental measurements, Chemical Engineering Research and Design 89 (2011) 2024–2037.
[22] R. Menter, Two-equation eddy-viscosity turbulence models for engineering applications, AIAA Journal 32 (8) (1994) 269–289.
[23] Fluent, Fluent 6.3 User's Guide, ANSYS Corporation, 2006.
[24] ASHRAE, Handbook of Fundamentals, American Society of Heating, Refrigerating and Air-Conditioning Engineers, 2005.
[25] H. Xie, J. Wang, T. Xi, Y. Liu, Thermal conductivity of suspensions containing nanosized SiC particles, International Journal of Thermophysics 23 (2) (2002) 571–580.
[26] J. Leitner, D. Sedmidubsky, B. Dousova, A. Strejc, M. Nevriva, Heat capacity of CuO in the temperature range of 298.15–1300 K, Thermochimica Acta 348 (2000) 49–51.
[27] S. Khandekar, Y.M. Joshi, B. Mehta, Thermal performance of closed two-phase thermosyphon using nanofluids, International Journal of Thermal Sciences 47 (2008) 659–667.
[28] B.C. Pak, Y.I. Cho, Hydrodynamic and heat transfer study of dispersed fluids with submicron metallic oxide particles, Experimental Heat Transfer 11 (2) (1998) 151–170.
[29] S.-Q. Zhou, R. Ni, Measurement of the specific heat capacity of water-based Al_2O_3 nanofluid, Applied Physics Letters 92 (093123) (2008) 1–3.
[30] D.P. Kulkarni, R.S. Vajjha, D.K. Das, D. Oliva, Application of aluminium oxide nanofluids in diesel electric generator as jacket water coolant, Applied Thermal Engineering 28 (2008) 1774–1781.
[31] Y. Xuan, W. Roetzel, Conceptions for heat transfer correlation of nanofluids, International Journal of Heat and Mass Transfer 43 (2000) 3701–3707.
[32] A. Akbarinia, A. Behzadmehr, Numerical study of laminar mixed convection of a nanofluid in horizontal curved tubes, Applied Thermal Engineering 27 (2007) 1327–1337.
[33] J.A. Eastman, S.R. Philpot, S.U.-S. Choi, P. Keblinski, Thermal transport in nanofluids, Annual Review of Materials Research 34 (2004) 219–246.
[34] J. Buongiorno, Convective transport in nanofluids, ASME Journal of Heat Transfer 128 (2006) 240–250.
[35] H. Angue Mintsa, G. Roy, C.T. Nguyen, D. Doucet, New temperature dependent thermal conductivity data for water-based nanofluids, International Journal of Thermal Sciences 48 (2009) 363–371.
[36] C.H. Chon, K.D. Kihm, S.P. Lee, S.U.-S. Choi, Empirical correlation finding the role of temperature and particle size for nanofluid (Al_2O_3) thermal conductivity enhancement, Applied Physics Letters 87 (153107) (2005) 1–3.
[37] J. Buongiorno, D. Venerus, N. Prabhat, T. McKrell, J. Townsend, R. Christianson, V. Tolmachev, P. Keblinski, et al., A benchmark study on the thermal conductivity of nanofluids, Journal of Applied Physics 106 (2009) 094312.
[38] M. Corcione, Rayleigh-Bénard convection heat transfer in nanoparticle suspensions, International Journal of Heat and Fluid Flow 32 (2011) 65–77.
[39] W.J. Tseng, K.-C. Lin, Rheology and colloidal structure of aqueous TiO_2 nanoparticle suspensions, Materials Science and Engineering A 355 (2003) 186–192.
[40] C.T. Nguyen, F. Desgranges, G. Roy, N. Galanis, T. Maré, S. Boucher, H. Angue Mintsa, Temperature and particle-size dependent viscosity data for water-based nanofluids – hysteresis phenomenon, International Journal of Heat and Fluid Flow 28 (2007) 1492–1506.
[41] S.V. Patankar, Numerical heat transfer and fluid flow, Hemisphere (1980).
[42] J.C. Tannehill, Computational Fluid Mechanics and Heat Transfer, Taylor and Francis, 1997.
[43] M. Behnia, S. Parneix, Y. Shabany, P.A. Durbin, Numerical study of turbulent heat transfer in confined and unconfined impinging jets, International Journal of Heat and Mass Transfer 20 (1999) 1–9.
[44] A.K. Colaciti, L.M. Valdés López, H.A. Navarro, L. Cabezas-Gómez, Numerical simulation of a radial diffuser turbulent airflow, Applied Mathematics and Computation 189 (2007) 1491–1504.
[45] N. Gao, D. Ewing, Investigation of the effect of confinement on the heat transfer to round impinging jets exiting a long pipe, International Journal of Heat and Fluid Flow 27 (2006) 33–41.
[46] D. Lytle, B. Webb, Air jet impingement heat transfer at low nozzle-plate spacings, International Journal of Heat and Mass Transfer 37 (1994) 1687–1697.
[47] D. Colucci, R. Viskanta, Effect of nozzle geometry on local convective heat transfer to a confined impinging air jet, Experimental Thermal and Fluid Science 13 (1) (1996) 71–80.

[48] P. Moller, Radial flow without swirl between parallel discs, The Aeronautical Quarterly 14 (1963) 163–186.
[49] M. Tabatabai, A. Pollard, Turbulence in radial flow between parallel disks at medium and low Reynolds numbers, Journal of Fluid Mechanics 185 (1987) 483–502.
[50] S.P. Jang, S.U.-S. Choi, Cooling performance of a microchannel heat sink with nanofluids, Applied Thermal Engineering 26 (2006) 2457–2463.
[51] K. Agrawal, H. Varma, Experimental study of heat transfer augmentation versus pumping power in a horizontal R12 evaporator, International Journal of Refrigeration 14 (1991) 273–281.